Medical & Biological Engineering & Computing (2021) 59:301–313
https://doi.org/10.1007/s11517-020-02308-4

ORIGINAL ARTICLE

Theoretical evaluation of enhanced gold nanoparticle delivery to PC3 tumors due to increased hydraulic conductivity or recovered lymphatic function after mild whole body hyperthermia

Manpreet Singh[1] · Ronghui Ma[1] · Liang Zhu[1]

Received: 1 July 2020 / Accepted: 30 December 2020 / Published online: 11 January 2021

Abstract

The objective of this study is to investigate the effect of hyperthermia-induced improvement of hydraulic conductivity and lymphatic function on both tumoral IFP reduction and nanoparticle delivery to PC3 tumors. We developed a theoretical model for nanoparticle transport in a tumor incorporating Starling's law, Darcy's law, transient convection, and diffusion of chemical species in porous media, and nanoparticle accumulation in tumors. Results have shown that both mechanisms were effective to decrease the IFP at the tumor center from 1600 Pa in the control without heating to 800 Pa in tumors with whole body heating. IFP reductions not only elevate the nanoparticle concentration in the tumor, but also result in a more uniform nanoparticle concentration in the tumor than that in the control without heating. Due to the IFP reductions at the tumor center and/or local blood perfusion increases, the final amount of accumulated nanoparticles in the tumor increased by more than 35–95% when compared to the control without heating. We conclude that increases in the hydraulic conductivity and recovery of lymphatic functions are possible mechanisms that lead to IFP reductions and enhancement in nanoparticle deposition in PC3 tumors observed in our in vivo experimental studies.

Keywords Bioheat transfer · Nanoparticle delivery to tumor · IFP reduction · Transvascular flow

Nomenclature

D_{eff}	Diffusion coefficient of nanoparticles in the porous tumor, m^2/s
C	Concentration of nanoparticles in the porous tumor, mol/m^3
C_p	Concentration of nanoparticles in the capillaries of tumors, mol/m^3
p	Interstitial fluid pressure in the tumor, Pa
p_{blood}	Blood pressure in capillary, Pa
$V_{f,r}$	Interstitial fluid velocity in the radial direction, m/s
K_t	Hydraulic conductivity of the porous tumor, $m^2/Pa\ s$
S/V	Surface area of capillaries per unit volume of the tumor, 1/m
S_{LY}/V	Surface area of lymphatic vessels per unit volume of the tumor, 1/m
L_p	Hydraulic permeability of the capillary wall, m/Pa s
L_{LY}	Hydraulic permeability of the lymphatic vessel wall, m/Pa s
$\dot{M}_{\text{acc}}$	Accumulation rate of nanoparticles in the entire tumor, mol/s
M_{acc}	Amount of nanoparticle deposition in the tumor, mol
k_f	Deposition rate coefficient of nanoparticles attached to tumor cells, 1/s
p_{LY}	Lymphatic hydrostatic pressure, Pa
r	Coordinate in the radial direction in spherical coordinates, m
R	Radius of the tumor, m
t	Time, s

Greek symbols

ε	Porosity of the tumor
ϕ	Fluid source or sink term in Darcy's law,1/s
$\dot{C}$	Source or sink term of nanoparticles in porous media, $mol/m^3 \cdot s$
σ_t	Osmotic reflection coefficient for plasma proteins for tumors
σ_f	Filtration reflection coefficient through either the capillary or lymphatic vessel walls

✉ Liang Zhu
zliang@umbc.edu

[1] Department of Mechanical Engineering, University of Maryland Baltimore County, 1000 Hilltop Circle, Baltimore, MD 21250, USA

π	Osmotic pressure in the interstitial space of tumors, Pa
π_{blood}	Osmotic pressure in the capillaries of tumors, Pa
τ	Time constant, s

Subscripts

blood	Blood
LY	Lymphatic
acc	Accumulation

1 Introduction

Inefficacy of some cancer treatments is attributed to the tumor patho-physiological micro-environment that hinders delivery of therapeutic agents. Tumors exhibit differential mass transport characteristics, such as elevated interstitial fluid pressure (IFP), disorganized and irregular tortuous vessel networks, poor tumor perfusion, large distances between capillaries in the interstitium, fluid loss at the periphery, large affinity and heterogeneous binding, and a dense extracellular matrix (ECM) [1]. All these factors impair accumulation and penetration of targeting moieties inside the tumor interstitium. Furthermore, tumors have relatively disparate physiological factors, such as vascular permeability, interstitial diffusion coefficients, and hydraulic conductivity that often show non-uniform distribution, leading to inadequate uptake of therapeutic agents. High-molecular-weight drugs have difficulty entering the tumor interstitial space. On the other hand, low-molecular-weight agents may penetrate more deeply into tumors. However, they are often limited by their rapid elimination by blood flow and increased uptake into normal tissues. This increased uptake results in toxicity to normal tissues and decreases the drug pay-load rate [2].

Most therapeutic drugs are delivered to cancer patients via intravenous injections due to risks of tumor reseeding during the process of a direct intratumoral injection. Although vascular permeability in tumors is typically larger than that of normal tissues due to an irregular and loose structure of the neoplastic endothelium of tumor capillaries [3, 4], the passive transport involved in systemic injections has to overcome many barriers to achieve a drug concentration in the entire tumor above a desired therapeutic level. In addition, poorly perfused tumor regions, such as the tumor core, may not be exposed to the threshold therapeutic drug concentration.

Localized heating on tumors has been used to increase transvascular permeability and boost drug/nanostructure extravasation from tumor capillaries to the tumor interstitial space during systemic drug delivery [5–10]. It was suggested that the enhancement in permeability was due to an enlargement of vascular endothelial pore size in tumors after mild hyperthermia [5]. One paper reviewed the effectiveness of combined radiofrequency thermal ablation and found adjuvant IV liposomal doxorubicin with heating increased tumor destruction by 25–30% [6]. Those previous studies speculated that transient thermal damage to the endothelial cells or altered cellular homeostatic mechanisms would increase cellular or nuclear membrane permeability to drugs, leading to more intracellular drug uptake [7–10]. Other suggested mechanisms include increased blood flow to the tumors and IFP reduction by localized heating. In Leunig et al., elevating temperatures of melanoma tumors in Syrian golden hamsters by immersing the tumor in a water bath at 43 °C for 30–60 min significantly decreased tumoral IFP and slowed down the tumor growth rate [11]. They attributed the IFP reductions to heating-induced vascular damage in these tumors. Studies by Hauck et al. showed significantly enhanced delivery of chimeric ^{125}I-labeled 81C6 in gliomas implanted in mice after inducing a local hyperthermia at 41.8 °C for 4 h [12]. Since they did not observe significant IFP reductions [13], they speculated that the enhancement in drug delivery might be due to heating-induced local blood perfusion increases. A recent experimental study by Stapleton et al. [14] reported reduced IFPs in human breast tumors initially exhibiting high IFPs via a laser heating to elevate the tumor temperature to 42 °C for 20 min. The local heating to tumors enhanced bulk accumulation of liposomes in the tumors [14]. However, in Lammers et al. [15], localized heating via immersing tumor-bearing limbs of rats into a warm water bath for 1 h showed a statistically significant increase in copolymer delivery in one of the three studied tumor groups when compared to the control without heating.

Furthermore, mild whole body hyperthermia has been implemented to increase nanoparticle delivery to tumors. A study demonstrated successful visualization of an endothelial lining gap induced by whole body hyperthermia (41 °C for 30 min) and enhancement in large-sized (~ 87 nm dia.) liposome extravasation and penetration into the interstitial space up to 27.5 μm from the vessel wall [16]. The effect of whole body hyperthermia on IFP reduction was first evaluated by Sen et al. and Winslow et al. on murine colon tumors, murine melanomas, and human head and neck tumors implanted in mice [17, 18]. They placed the mice in a heating chamber to induce mild whole body hyperthermia for several hours. Correlations were established among IFP reductions, increases in local tumoral blood perfusion, reductions in tumor hypoxia, and enhanced liposome extravasation from tumor capillaries.

Similarly, a recent study by our group illustrated the effectiveness of using mild whole body hyperthermia (40 °C) to lower IFP and enhance nanoparticle delivery to PC3 tumors implanted in mice [19]. In that experiment, nude mice with implanted PC3 tumors on their flank were divided into two groups, with or without 1-h whole body hyperthermia. A previously developed gold nanofluid was injected into the tail vein of mice after the whole body heating. The IFPs at the

tumor center and periphery were measured before the heating, right after the heating, 2 h post heating, and 24 h post heating. Later, the tumors were resected 24 h post heating to quantify nanoparticle deposition using microCT. Statistically significant IFP reductions of 45% right after heating, 47% 2 h after heating, and 52% 24 h after heating were observed in the whole body hyperthermia mouse group. MicroCT analyses of the resected tumors illustrated that nanoparticles were more concentrated near the tumor periphery rather than at the tumor center, and suggested an overall 42% more nanoparticle delivery in the heating group than that in the control group without heating. It was speculated that the observed IFP reductions might be due to increases in hydraulic conductivity of porous tumors or improvement of functional lymphatic vessels in tumors as a result of heating. A larger hydraulic conductivity of a porous tumor would decrease the flow resistance and allow the fluid to move towards the tumor periphery. Additionally, functional lymphatic drainage may contribute by significantly reducing the amount of solute present in the tumor, as fluids and solutes are reabsorbed from the tumor tissue by lymphatic vessels. Our experimental studies also showed sustained increases in the blood perfusion rate in both the mouse body and tumor for 24 h after the implemented 1-h whole body hyperthermia, thus allowing more nanoparticles to be delivered to the PC3 tumors [20].

Transport of fluid, macromolecules, and nanoparticles in tumors has been studied via mathematical simulations since the 1980s. Typically, the tumor was treated as a porous medium and the transvascular fluid/particle transport was modeled as a continuum. The mathematical model was first introduced by Baxter and Jain [4] to model the radial fluid transport in a spherical tumor as distributed fluid sources and sinks, and macromolecule concentration distribution in tumors was determined by solving a convection/diffusion equation with a source term for extravasation of drug from blood vessel and a sink term for extravascular binding. The effects of increasing hydraulic conductivity of the microvessels of a tumor on drug/particle concentration distribution were investigated by El-Kareh and Secomb in 1995 [21]. It was reported that an optimal value of microvessel hydraulic conductivity can maximize the infiltration rate of drug at the tumor center, and this critical value is more dependent on the tumor size than the shape. Most of the theoretical simulation in past years was largely focused on evaluation of the role played by cell uptakes and particle elimination from the interstitial space. The cell uptake of nanocarriers in tumor cells was estimated using a two-compartment exchange model connected to the interstitial compartment [14]. In this approach, the interaction between tumor cells and nanoparticles is the result from binding of receptors and ligands, a reversible reaction process. Further, in Su et al. [22], a microscopic particle tracking model was developed in a cell-fluid compartment to evaluate the collective effect of nanoparticle attachments to tumor cells. The averaged deposition rate coefficient obtained from the particle tracking model was later used in a continuum model as a particle sink term to determine nanoparticle distribution during and after an intratumoral injection of nanofluid in a porous tumor. Stapleton et al. [23] presented a theoretical framework based on pressure-driven fluid flow across blood vessels and through the tumor interstitium to describe liposome transport in solid tumors. The model was validated by computed tomography measurements of accumulation of liposomes in three preclinical tumor models. Their study predicted inter-subject and intra-tumoral variations in the enhanced permeability and retention effect. Stapleton et al. [14] performed simulations in a high IFP tumor and showed that decreasing steady-state IFP by only 1% is sufficient to increase nanotherapeutic exposure. In this study, simulation was also performed to examine the effects of temporarily decreasing or spatiotemporally modulating IFP on nanotherapeutic exposure. The study reported that the transient effects on fluid dynamics in tumors with high IFPs were a possible mechanism of improving drug delivery. In a recent study by Chakraborty et al. [24], the authors proposed a mixed model in which two parallel cylindrical blood vessels and a lymph vessel are embedded in bulk tissue. The model combines both individual blood/lymphatic vessels and the continuum approach of convection/diffusion in the rest of the tumor region, and investigated nanoparticle transport as a function of the solute size, the intercapillary separation, and the flow direction in microvessels. It represents an advancement in accurate modeling of nanoparticle delivery and deposition in porous tumors.

In this study, we adopted the theoretical approaches from previous studies to model gold nanoparticle transport in tumors, to evaluate to what extent increased hydraulic conductivity or improvement in lymphatic functions in porous tumors contributes to the increase in gold nanoparticle delivery. It examines the roles played by flow resistance and lymphatic drainage in promoting nanoparticle extravasation from the tumor capillary, nanoparticle diffusion, and nanoparticle deposition in PC3 tumors. The experimentally measured IFP values at the tumor center were used to determine the hydraulic conductivity of the porous PC3 tumor or the permeability for transvascular fluid transport across lymphatic vessels. Using a transport model of nanoparticles in a porous medium and data from a previously developed nanoparticle trajectory model, we quantified the increased nanoparticle deposition in tumors after tumor-bearing mice are subjected to whole body hyperthermia and compared the results to experimental measurements.

2 Mathematical formulation

A tumor is modeled as a porous medium in a sphere of 10 mm in diameter [19]. The size of the tumor is selected based on the

same average transverse diameter of the PC3 tumors used in our previous study [19]. The characteristic macroscopic length scale of a tumor (10 mm) is several orders of magnitude larger than the typical length scale of the inter-capillary distance ~ 50–100 μm. Hence, mass and fluid transport in the tumor is considered in a continuous porous medium. The interstitial fluid is assumed as a Newtonian fluid and is intrinsically incompressible. The tumor is modeled as spatially homogeneous with uniform biological and physical properties, shown in Fig. 1. All the variables are considered one dimensional (1-D) in the radial direction in a spherical coordinate system.

The fluid extravasation from the capillaries or to the lymphatic vessels is considered a fluid source or a fluid sink term expressed as the volume of fluid to or from the interstitial space per unit time per unit volume of the tumoral tissue, expressed by Starling's law [25],

$$\phi_{\mathbf{blood}}-\phi_{\mathbf{LY}} = \left(\frac{L_p S}{V}\right)[p_{\mathbf{blood}}-p-\sigma_t(\pi_{\mathbf{blood}}-\pi)]-\left(\frac{L_{\mathbf{LY}}S_{\mathbf{LY}}}{V}\right)[p-p_{\mathbf{LY}}] \quad (1)$$

The fluid source term is determined by the pressure difference between the capillary pressure p_{blood} and IFP p, the effective osmotic pressure difference, and the density of the capillary in tumor tissue. The fluid sink term is related to the difference between IFP and lymphatic pressure p_{LY}. The hydraulic permeabilities of the capillary wall L_{p} and the lymphatic vessel wall L_{LY} in the tumor and the vasculature surface area per unit tissue volume S/V are also showing in the fluid source term and sink term, respectively. The source and sink terms are used in the mass conservation equation in a porous medium, to determine the interstitial fluid velocity in the radial direction $V_{f,r}$, governed by Darcy's law [26],

$$\frac{d(\varepsilon V_{f,r})}{dr} = \phi_{\mathbf{blood}}-\phi_{\mathbf{LY}} \quad (2a)$$

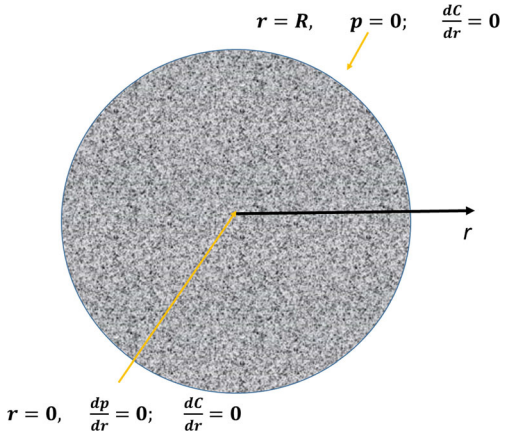

Fig. 1 Schematic diagram of the modeled tumor and the boundary conditions

$$\varepsilon V_{f,r} = -K_t\frac{dp}{dr} \quad (2b)$$

where ε is the porosity of the tumor, and K_t is the hydraulic conductivity of the porous tumor, which is related to the flow resistance in the porous medium.

The general equation for molecular transport in the tumor tissue is based on the conservation law for chemical species in porous media [25, 26], and the governing equation of the nanoparticle concentration field is expressed as:

$$\frac{\partial C}{\partial t} = D_{\mathbf{eff}}\frac{1}{r^2}\frac{\partial}{\partial r}\left(r^2\frac{\partial C}{\partial r}\right)-\frac{d}{dr}(V_{f,r}C) + \dot{C}_{\mathbf{blood}}-\dot{C}_{\mathbf{LY}}-k_f C \quad (3)$$

where C is the local nanoparticle concentration based on the tissue volume, D_{eff} is the effective diffusion coefficient of the nanoparticles in the porous medium, and $\dot{C}_{\mathbf{blood}}$ and $\dot{C}_{\mathbf{LY}}$ are the nanoparticle source term and sink term representing the rate of nanoparticle transport across a capillary wall or across a lymphatic vessel wall, respectively,

$$\dot{C}_{\mathbf{blood}} = \phi_{\mathbf{blood}}(1-\sigma_f)C_p \text{ and } \dot{C}_{\mathbf{LY}} = \phi_{\mathbf{LY}}(1-\sigma_f)C \quad (4)$$

where σ_f is the filtration reflection coefficient, and C_p is the nanoparticle concentration in the plasma of capillaries. Equation 4 assumes that diffusion is much smaller than advection [25]. Due to nanoparticle deposition in the tumor and clearance by other organs such as the liver, spleen, and kidneys, nanoparticle concentration in blood plasma decreases with time. In this study, it is assumed that the decay of C_p follows an exponential function with a time constant τ,

$$C_p(t) = C_{p,0}\exp\left(-\frac{t}{\tau}\right) \quad (5)$$

where $C_{p,0}$ is the initial peak concentration of the nanoparticles in the plasma following the intravenous injection of a nanofluid and mixing with the blood in the circulation system in the mouse.

In Eq. 3, k_f is the deposition rate coefficient of the nanoparticles attached to tumor cells. Thus, the last term on the right side of Eq. 3 represents a nanoparticle sink to reduce the nanoparticle concentration in the interstitial fluid, therefore, limiting the diffusion depth of the nanoparticles in tissue. Typically, nanoparticles suspended in fluid do not always follow the flow of fluid. There are many individual forces acting on individual nanoparticles, including van der Waals attractive force, electrostatic double-layer force, hydrodynamic drag force, lift force, buoyancy force, and Brownian motion [22, 27]. Van der Waals forces and Brownian motion may lead to particle deposition on the cell surfaces. We assume that a nanoparticle deposited on a cell surface stays on the cell surface and does not join the interstitial fluid again after its

attachment. In this study, k_f was determined via our developed microscale particle trajectory model [22, 27]. For the nanoparticles used in this study, it was derived as

$$\boldsymbol{k_f}=\mathbf{0.023}\ \left(\boldsymbol{s^{-1}}\right) \tag{6}$$

Hyperthermia may modify tumor environment and lead to reduced tortuosity. The reduced tortuosity would then increase the interstitial velocity and subsequently change the particle deposition rate coefficient. For tumors with a porosity as low as 0.2, the reduced tortuosity will not have a significant influence on the path line of nano-sized particles over micro-sized cells. We assume that it is reasonable to use a constant deposition rate coefficient value during hyperthermia. Further, nanoparticles used in target drug delivery as carriers to enhance drug delivered to the tumor are usually coated with agents to facilitate bonding and internalization. The dissociation and resuspension of the nanoparticles is therefore considered negligible. Additionally, internationalized nanoparticles do not change the overall distribution of the particles in the tumor and nanoparticle clearance is not included in the model.

The time-dependent accumulation rate of nanoparticles in the tumor, $\dot{M}_{\mathrm{acc}}(t)$, is the integration of the last term on the right side of Eq. 3 over the entire tumor as

$$\dot{\boldsymbol{M}}_{\mathbf{acc}}(\boldsymbol{t}) = \iiint_{\mathbf{tumor}} \boldsymbol{k_f} * \boldsymbol{C}(\boldsymbol{r},\boldsymbol{t})\boldsymbol{d}\mathbf{Volume} \tag{7}$$

Finally, the amount of nanoparticle deposition in the tumor is determined by integrating $\dot{M}_{\mathrm{acc}}(t)$ over time as

$$\boldsymbol{M}_{\mathbf{acc}}(\boldsymbol{t}) = \int_0^t \dot{\boldsymbol{M}}_{\mathbf{acc}}(\boldsymbol{s})\boldsymbol{ds} \tag{8}$$

Equations 2a and 2b can be combined into a governing equation for the pressure field in the interstitial fluid space, p. Boundary conditions required for solving the pressure field are a prescribed pressure at the tumor periphery as zero and zero pressure gradient at the tumor center due to symmetry [21]. For the nanoparticle concentration field C, the initial condition is a zero nanoparticle concentration distribution in the tumor. The boundary conditions are zero concentration gradients at both the center ($r = 0$) due to symmetry and the periphery ($r = R$) due to the dominant role played by advection. They are expressed as:

$$\boldsymbol{r}=\mathbf{0},\qquad \frac{\boldsymbol{dp}}{\boldsymbol{dr}}=\mathbf{0};\qquad \frac{\boldsymbol{dC}}{\boldsymbol{dr}}=\mathbf{0} \tag{9a}$$

$$\boldsymbol{r}=\boldsymbol{R},\qquad \boldsymbol{p}=\mathbf{0};\qquad \frac{\boldsymbol{dC}}{\boldsymbol{dr}}=\mathbf{0} \tag{9b}$$

In previous animal experimental studies by our group [19, 20], we observed that the IFPs at the center of PC3 tumors after 1-h whole body hyperthermia were approximately half of that in the tumors without heating. The experiments also demonstrated increases in the blood perfusion rate in the tumor by 25% on average after heating. The observed IFP reductions and the increases in blood perfusion rate were maintained for at least 24 h after heating. In this study, simulations are conducted to evaluate the roles played by either increases in the hydraulic conductivity of the porous tumor or improvement of the lymphatic functions in the tumor. In addition, the blood perfusion rate increase in the tumor is modeled as a plasma pressure (p_{blood}) increase in the tumor capillaries. One can model the blood flow from capillaries to the venules as a simple flow-resistant network. Assuming that the hydrostatic pressure in the venules is zero and the flow resistance of the blood vessel network is unchanged, one can determine that the hydrostatic pressure in the tumor capillaries (p_{blood}) would increase by 25% if the local blood perfusion rate is elevated by 25%.

As shown in Table 1, five cases are simulated in this study. Case A (the control) is for a tumor without heating, where p_{blood} is assigned as 3233 Pa (24 mmHg) and there is no lymphatic transvascular flow, and the hydraulic conductivity of the porous tumor K_t is first adjusted to match our experimental measurement of IFP at the tumor center as 1600 Pa. Cases B1 and B2 examine the role played by K_t in IFP reduction by adjusting its value to match the experimentally measured IFP of 800 Pa at the tumor center. The impact of recovery of lymphatic function in the tumor is evaluated in cases C1 and C2, where the K_t is unchanged as in the control while $L_{\mathrm{LY}}S_{\mathrm{LY}}/V$ shown in Eq. 1 is adjusted so that the predicted IFP at the tumor center is consistent with our experimental measurement of 800 Pa. In cases B2 and C2, the hydrostatic pressure in the tumoral capillary is elevated to account for the 25% increase in the blood perfusion rate in the tumor. Although enhanced hydraulic conductivity and recovery of lymphatic function may occur simultaneously, their roles are examined separately in this study to achieve a better understanding of their individual contributions to nanoparticle delivery.

The coupled equations described above were discretized based on mass, momentum, and concentration conservations. MATLAB codes were written to simulate the steady-state fluid velocity and pressure fields as well as the transient concentration field in the tumor. Explicit scheme was used for the simulation of the transient process of nanoparticle concentration distribution in the tumor. The numerical simulation results have been compared to an analytic solution derived for the pressure distribution in the radial direction. It was found that the numerical simulation results of the pressure fields agree very well with the prediction by the analytical solutions, with deviations less than 1%. The total simulation was conducted over a long duration until the nanoparticle concentration in the capillary plasma was less than 1% of its peak value. Result sensitivity to the spatial step and time step in the numerical simulation was examined. Decreases in the spatial

Table 1 Five cases in the simulation. # denotes adjusted parameters

	Case A—control	Case B1	Case B2	Case C1	Case C2
p_{blood} (Pa)	3233	3233	4041	3233	4041
$p(0)$ (Pa)	1600	800	800	800	800
$p(R)$ (Pa)	0	0	0	0	0
K_t (m^2/Pa s)	9.96×10^{-13}	$2.73 \times 10^{-12\#}$	$3.45 \times 10^{-12\#}$	9.96×10^{-13}	9.96×10^{-13}
$L_{LY}S_{LY}/V$ (1/Pa s)	0	0	0	$6.37 \times 10^{-7\#}$	$1.09 \times 10^{-6\#}$

step or time step by 50% resulted in a change of less than 1% in the final results of nanoparticle accumulation.

3 Results

In our previous experiments, 0.2 ml of a gold nanofluid (AuNP-PPI-CO_2H, 10 mgAu/ml) was injected into the tail vein of mice weighing approximately 25 g, and a total blood volume inside the mouse was 1.46 ml [19, 20]. The total amount of gold delivered to the mouse is determined as 1.015×10^{-5} mol. The initial nanoparticle concentration in the plasma can be calculated as 6.952 mol/m^3. In this study, we assume that C_p decays with a time constant τ equal to 5193 s. This is equivalent to a half time of clearance in the blood stream as 3600 s, similar to that reported in previous studies [28]. The value of the deposition rate coefficient k_f was estimated based on our previously developed particle trajectory model, with the size of the developed AuNP-PPI-CO_2H nanoparticles as 28 nm in diameter and surface zeta potential as − 30 mV [21, 22]. The values of all these physiological parameters used are summarized in Table 2 [4, 19, 20, 22, 24, 27, 29–32].

Figure 2 illustrates the pressure distribution in the radial direction in the interstitial fluid space. It clearly demonstrates higher IFPs at the tumor center than that at the periphery, similar to experimental observations. For the tumor without heating (case A), the hydraulic conductivity K_t of the porous medium is first adjusted to 9.96×10^{-13} (m^2/Pa s) so that the tumor center IFP is 1600 Pa. In cases B1 and B2, the hydraulic conductivity has to be 2.74 times (case B1, $K_t = 2.73 \times 10^{-12}$ m^2/Pa s) or 3.46 times (case B2, $K_t = 3.45 \times 10^{-12}$ m^2/Pa s) of the value in the control (case A) to match the IFP reduction to 800 Pa at the tumor center after whole body hyperthermia. Using the same hydraulic conductivity of the control, one finds that improvement in the lymphatic function would also result in the same IFP reduction. Shown in Fig. 2, the improvement of the lymphatic function, i.e., $L_{LY}S_{LY}/V$, is changed from zero in case A to 6.37×10^{-7} 1/Pa s and 1.09×10^{-6} 1/Pa s, respectively, so that p at the tumor center matches the IFP value of 800 Pa. Note that the pressure profiles of cases B1 and cases B2 are almost the same. In cases C1 and C2, the hydrostatic pressures in the tumoral capillary are slightly different at the tumor periphery. Comparing the two mechanisms, the pressure fields in the central region of the tumor are more uniform in the radial direction of the tumor in cases C1 and C2 than those in cases B1 and B2.

The interstitial fluid flow profiles in the radial direction are plotted in Fig. 3. The interstitial fluid motion is induced by the fluid sources and sinks of the transvascular and translymphatic flows. The high strength of the fluid sources towards the tumor periphery leads to large fluid velocities towards the tumor surface. In cases B1 and B2 with a larger hydraulic conductivity than the control, fluid moves through the interstitial space much faster, approximately 31% and 90% higher at the tumor periphery, respectively, than that in the control.

In case C1 and case C2 with improvement of lymphatic function, the resulting velocity profiles in the radial direction are quite different from those in case B1 and case B2. As illustrated in Fig. 3, due to the additional fluid sink by the lymphatic drainage, the resulting maximal velocity in the radial direction in case C1 decreases by 27% from the control. In case C2, although the lymphatic drainage decreases fluid flow

Table 2 Parameters used in the simulations in SI units with references

Trans-capillary flow	Trans-lymphatic flow	Porous tumor
π_{blood} [29]: 2660 Pa	p_{LV} [4]: 0 Pa	$p(0)$ [19, 20]: 1600 or 800 Pa
π [29]: 1330 Pa		$p(R)$: 0 Pa
σ_t [4, 30]: 0.82	σ_f [4, 24, 31]: 0.9	R: 0.005 m
L_p [4]: 2.1×10^{-11} m/Pa s	$L_{LV}S_{LV}/V$: adjustable	K_t: adjustable
S/V [4]: 20000 1/m		ε [4, 8]: 0.2
$C_{p,0}$ [19]: 6.952 mol/m^3		D_{eff} [32]: 9.57×10^{-12} m^2/s
τ: 5193 s		k_f [22, 27]: 0.023 1/s

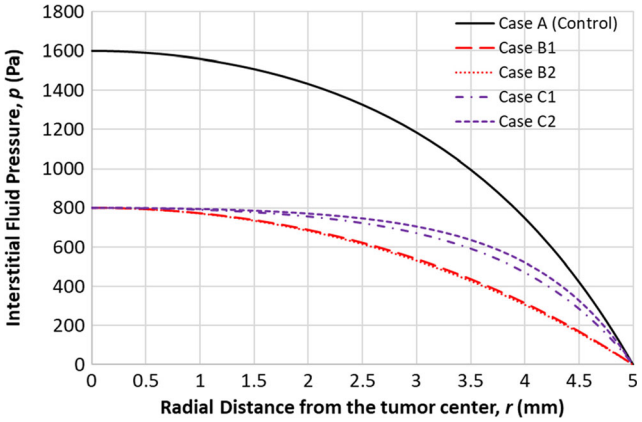

Fig. 2 Interstitial fluid pressure distributions in the radial direction for all five cases

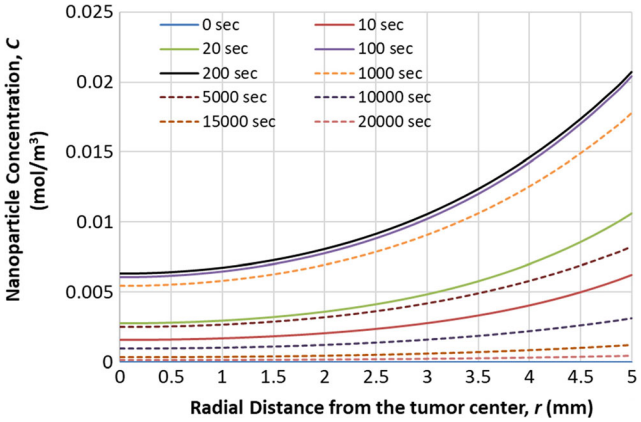

Fig. 4 Elevations and decays of nanoparticle concentration distribution in the radial direction in the tumor without heating

in the radial direction, its effect is countered by the increase in p_{blood}. In case C2, the resulting maximal velocity decreases by only 12% from the control. The slight difference of velocity profile in cases C1 and C2 is primarily due to the relative contribution of the lymphatic drainage in the tumor region. As shown in Eq. 1, the lymphatic drainage is only dominant at the tumor central region, while it plays a very minor role at the tumor periphery where the IFP is almost the same as the lymphatic pressure p_{LY}. Note that in case C2, the fluid generated from the transcapillary flow is much larger than that in case C1. At the tumor periphery where the lymphatic drainage is diminishing, it leads to a slightly larger amount of fluid removed at the tumor periphery than that in case C1.

Figure 4 shows the transient nanoparticle concentration distribution in the tumor in the control case without heating (case A). Initially, the nanoparticle concentration is zero in the tumor. It gradually increases due to nanoparticle extravasation from the capillaries (the solid curves in Fig. 4). A peak concentration profile in the radial direction occurs after approximately 200 s. However, due to nanoparticle deposition in the tumor and clearance by other organs in the body, the nanoparticle concentration in the tumor starts to decrease with time (the dashed lines in Fig. 4). At approximately 20000 s (5.5 h), it is observed that less than 2% of the maximal nanoparticle concentration is in the tumor, implying negligible nanoparticle presence in the blood stream in the mouse body. The contribution of particle diffusion due to a non-uniform concentration field during the transient transport processes is at least one order of magnitude smaller than that due to advection.

The peak nanoparticle concentration profiles in the radial direction are illustrated in Fig. 5. The peak nanoparticle concentrations of all five cases occur at approximately 200 s. Overall, there are higher nanoparticle concentrations in the tumor periphery than in the center. In case A (the control without heating), the nanoparticle concentration at the tumor center is barely 30% of that at the tumor periphery (case A: 0.00655 mol/m^3 at the center vs 0.0216 mol/m^3 at the periphery). Figure 5 demonstrates the marked increase in the nanoparticle concentration in the tumor with whole body hyperthermia when the IFP at the center is smaller. The percentage of nanoparticle concentration at the center is more than 73% of that at the tumor periphery in case B1. The contribution of local blood perfusion rate in the tumor to nanoparticle delivery can be seen from the concentration profile in case B2,

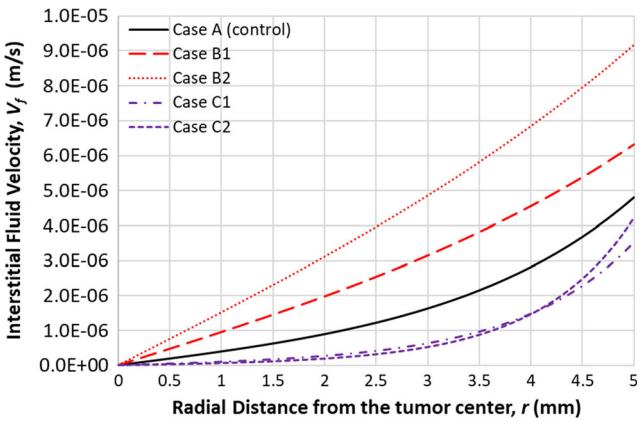

Fig. 3 Interstitial fluid velocity distribution in the radial direction for all five cases

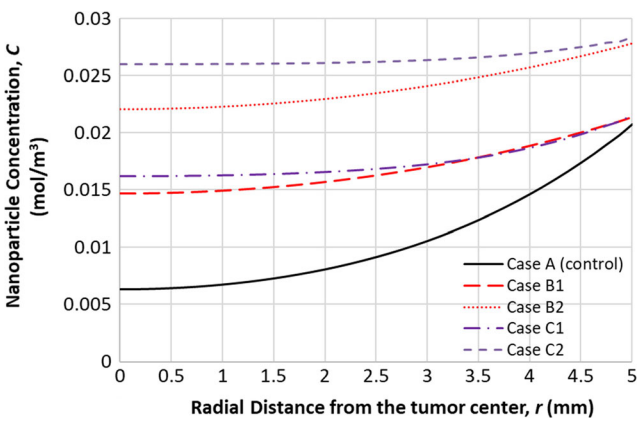

Fig. 5 Nanoparticle concentration distribution in the tumor at their peaks in all five cases

illustrating not only higher nanoparticle concentrations, but also more uniform nanoparticle concentrations in the tumor. Similar trends are observed in cases C1 and C2 with improvement of lymphatic drainage. Case C2 demonstrates the highest nanoparticle concentration among all five cases, with 0.0270 mol/m^3 at the center and 0.0294 mol/m^3 at the periphery. The nanoparticle concentration at the tumor center is more than 92% of that at the tumor center, suggesting an almost uniform nanoparticle concentration in the tumor in case C2.

Nanoparticle deposition in the tumor is directly proportional to the local nanoparticle concentration C and the deposition rate coefficient k_f (Eq. 3). Since k_f is assumed unchanged for all cases, the larger the local nanoparticle concentration, the higher the nanoparticle deposition rate on cell surfaces. From Fig. 5, one would expect to see more nanoparticles deposited on the tumor periphery than at the tumor center. This is also consistent with our experimental observations. Since whole body hyperthermia would significantly elevate nanoparticle concentration at the tumor center (Fig. 5), it would also help enhance nanoparticle delivery to the tumor center and result in a more uniform nanoparticle deposition in tumors.

Nanoparticles deposited on cell surfaces are assumed to stay on the cell surfaces and do not join the interstitial fluid again after their attachment. The total accumulated amount of nanoparticles would increase with time. Figure 6 illustrates an initial rise and later decay in the accumulation rate in the entire tumor, $\dot{M}_{\mathrm{acc}}(t)$, with time. Initially, $\dot{M}_{\mathrm{acc}}(t)$ is zero before the nanofluid injection. $\dot{M}_{\mathrm{acc}}(t)$ almost doubles its value at t = 100 s from that at t = 20 s. From t = 100 s to the quasi-steady state at 200 s, the accumulation rate changes only slightly. Later, the accumulation rate decays due to decreases in the nanoparticle concentration in the capillary plasma. The peak accumulation rates, $\dot{M}_{\mathrm{acc}}(t)$, in the entire tumor in the control without heating is 1.72×10^{-10} mol/s. In case B1 and case C1 with heating, the accumulation rate increases by 30% from the control. When the local blood perfusion rate increase is considered in case B2 and case C2, it enhances the total accumulation rate in the tumor by 78% and 88% from that without heating, respectively. After the peak, the accumulation rate decays with time. They decrease to 50% of their peak values after approximately 4000 s.

The quantity of nanoparticles delivered and deposited in the tumor is estimated by $M_{\mathrm{acc}}(t)$. Shown in Fig. 7, the curves corresponding to all cases illustrate a rising trend with time. It takes 1 h to reach 50% and 3.05 h to reach 90% of their values at the end of the simulation. In the control without heating (case A), the final amount of nanoparticle deposition is approximately 8.35×10^{-7} mol, which is 8.1% of the total amount of nanoparticles delivered to the blood stream via the tail vein. However, with the enhanced hydraulic conductivity of the porous tumor (K_t), the final amount of nanoparticle deposition increases to 1.12×10^{-6} mol in case B1 and further to 1.54×10^{-6} mol in case B2 when considering the local blood perfusion rate increases in the tumor. Examining the effect of improvement in lymphatic drainage, one observes slightly larger nanoparticle deposition increases, with 1.13×10^{-6} mol in case C1 and 1.63×10^{-6} mol in case C2. In other words, compared to the control with only 8.1% of the total amount of the nanoparticles captured by the tumor, enhanced conductivity or improved lymphatic function would boost the percentage of nanoparticles captured by the tumor to 11–16% of the injected nanoparticles in the circulatory system.

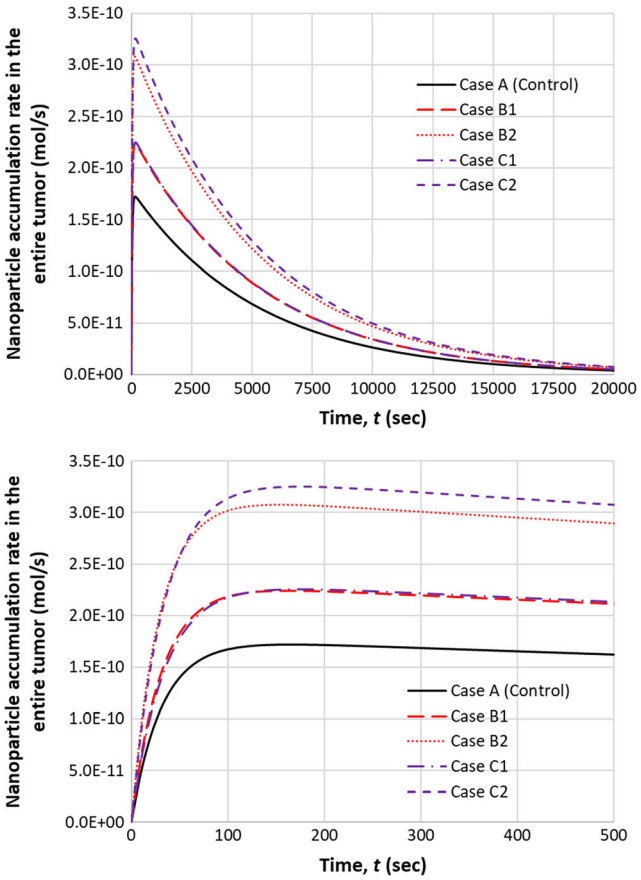

Fig. 6 Rate of nanoparticle accumulation in the entire tumor at various time instants, $\dot{M}_{\mathrm{acc}}(t)$. The top panel provides the transient process of the entire simulation duration, while the bottom panel shows details in the first 500 s

4 Discussion

In our previous experiments, IFPs were measured at two tumor locations, one was at the center of the tumor, and the other was at a tumor peripheral location halfway between the center and the surface. The measured average IFP value at the periphery site was approximately 90% of that at the tumor center in the tumor group without whole body hyperthermia. Note that the theoretical prediction of the IFP at the periphery

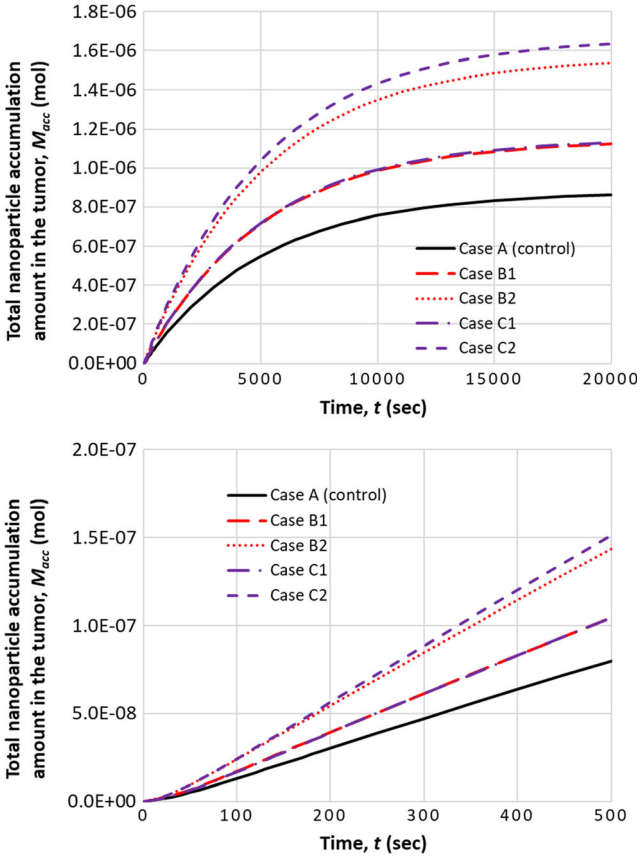

Fig. 7 The amount of nanoparticle deposition in the tumor verse time. The top panel provides the transient process of the entire simulation duration, while the bottom panel shows details in the first 500 s

location (r = 2.5 mm) in the theoretical simulation is smaller, approximately 84% of that at the tumor center, implying a good agreement with the experimental measurements. In the tumor group after 1-h whole body hyperthermia, experimental measurements of the IFP at the tumor periphery indicated that the average IFP values were 92% of the IFPs at the center right after the whole body hyperthermia, and 91% of the IFPs at the center 2 h post heating. Examining the radial profiles of the IFP in cases B1, B2, C1, and C2, one finds that the theoretically predicted IFP at the periphery location of r = 2.5 mm varies from 75% of that at the center in cases B1 and B2 to 88% in cases C1 and C2. The close agreement between the ratio predicted by the theoretical simulations and the in vivo experimental results renders some credibility of the current study.

It has been well known that the IFPs of most solid tumors are elevated. The elevation in IFP spreads through the entire tumor except at the tumor periphery where it drops abruptly. At the tumor center, it has been reported that IFP can be as high as 60 mmHg [32]. If one considers that the driving force for transcapillary flow is the difference between plasma pressure in the capillary and IFP, elevated IFPs in the interstitial fluid space would greatly decrease or even abolish transcapillary flow. Thus, it is not a surprise to see that most cancer cells are exposed to a very low drug concentration, oftentimes below the minimal drug concentration needed to achieve treatment efficacy. Previous studies have also shown that cancer patients having tumors with higher IFPs often had poorer prognosis and higher recurrence rates [33, 34]. In addition, tumors at later growth stages typically have a blood supply smaller than that in normal tissue. Some tumors can survive in hypoxic conditions with little O_2 requirements. In thermal ablation that causes irreversible thermal damage to tumor cells, it is actually advantageous to induce higher temperature elevations at the tumor site due to its small blood perfusion rate [35]. However, this method inhibits delivery of therapeutic agents. As mentioned earlier, the small blood perfusion rate in tumors is often associated with a low hydraulic pressure in tumor capillaries. This would further decrease the driving force for transcapillary flow of drug delivery. Therefore, in theory, any approach involving reduced IFPs and/or increased blood supply to tumors would greatly augment delivery of therapeutic agents to tumors. Shown in our previous microCT study of nanoparticle distribution in resected tumors with or without 1-h whole body hyperthermia in mice, the total mass of gold nanoparticles in PC3 tumors increased by 48% in tumors with heating from that in the control without heating [19]. The simulation results of the deposition of nanoparticles using the experimentally measured IFP values demonstrated increases of 35–95% from the control, suggesting a good agreement with the experimental data. Furthermore, previous microCT data demonstrated a lower concentration of nanoparticles at the center of PC3 tumors, and our theoretical simulation showed the deposition at the center is barely 30% of that at the tumor periphery in the control. Consistent with the experimental results after the mice were exposed to 1-h whole body hyperthermia, the predicted nanoparticle distribution inside the tumors is more uniform, as more nanoparticles are deposited in the central region of tumors.

In this study, we simulate nanoparticle transport in a porous tumor to evaluate multiple physical factors that affect the nanoparticle delivery, such as interstitial fluid flow, decreasing amount of nanoparticles in the systemic blood circulation, nanoparticle extravasation from the capillaries, nanoparticle advection in the interstitial medium, and possible nanoparticle deposition on tumor cells. As such, this model not only predicts the evolution of nanoparticle accumulation in the tumor over time, but also provides the radial nanoparticle concentration distribution in the tumor. The good agreement between the enhancement in nanoparticle deposition rate in the modeled tumor and our previous in vivo experimental observations suggests that an increase in hydraulic conductivity of a porous tumor is one possible mechanism that results in IFP reductions, thus, leading to the enhanced nanoparticle delivery. This may be related to heating-induced structural changes

in the extracellular matrix (ECM). In general, the network of collagen fibers in the extracellular matrix of tumors is much denser and thicker than that in normal tissue [1]. Tumors also have increased numbers of fibroblasts that bind to collagen fibers and inflammatory cells as compared to normal tissue [36]. We speculate that whole body hyperthermia makes the connective tissue less rigid and/or promotes more release or removal of some bio-chemicals that originally promoted high IFPs in tumors. It is also possible that whole body hyperthermia decreases tortuosity of interstitial fluid pathways and/or forms new connections among originally isolated interstitial fluid pockets. However, more experimental studies are needed to verify those specific mechanisms, including using experimental techniques to measure hydraulic conductivity in porous tumors before and after whole body hyperthermia.

IFPs in tumors may also decrease back to normal with approaches to normalize blood vessels. Previous experimental studies have shown the effectiveness of using anti-VEGF (vascular endothelial growth factor) therapy to modify the immature vessels and to improve structures of the ECM [37]. PDGF (platelet-derived growth factor) antagonists were used to decrease contraction of stromal fibroblasts and interactions with ECM [38]. Another pro-inflammatory factor PGE_1 (prostaglandin E_1) demonstrated its effect on reductions of contractility of stromal fibroblasts in tumors [39]. However, it is unlikely that those mechanisms played roles in the current study since normalization of blood vessels in tumors is likely to decrease permeability of the leaky capillaries, thus leading to reduction of transcapillary flow.

Lymphatic vessels are absent or non-functional in tumors [36], leading to inefficient drainage of fluid and interstitial proteins from the tumor tissue in early stages of tumor growth. In the current theoretical simulation, we assume the existence of lymphatic vessels in PC3 tumors, but high solid stress in tumors may compress those lymphatic vessels. Whole-body hyperthermia may modify ECM, and decrease solid stress in tumors. The originally collapsed lymphatic vessels may subsequently reopen due to the reduction of solid stress. Heating itself may directly result in opening of lymphatic vessels. In physical therapy, taking a hot shower has been recommended to patients in order to remove stagnant lymphatic fluid in tissues, as lymphatic vessels dilate with elevated temperatures [40]. As shown in the theoretical simulation, recovered lymphatic function in tumors is an effective mechanism to promote fluid drainage. For the same IFP reduction at the tumor center, improvement in the lymphatic function would lead to more uniform nanoparticle concentration elevations across the tumor region and higher nanoparticle deposition in the tumor than that caused by increases in hydraulic conductivity of porous tumors. One thing needs to be pointed out is the connection between increased lymphatic drainage and tumor metastasis suggested by previous studies [41] in late growth stage of tumors. Using MRI imaging technique, tumor invasiveness were associated with increased lymphatic drainage area in human breast cancer models [42]. Similarly, more experimental studies are warranted to provide experimental evidence of functional lymphatic systems in PC3 tumors after whole body hyperthermia, especially with real-time monitoring or visualization of lymphatic vessels with advanced imaging techniques.

There are several limitations of the developed theoretical model. The spherical tumor could be replaced by a more realistic model constructed from imaging scans [43]. Our simulation results are based on an assumption of uniform blood perfusion rate in tumors in terms of the uniform surface area of capillaries/lymphatic vessels per unit tumor volume. The theoretical model does not consider the much lower blood perfusion rate in the tumor's central region, especially in tumors at their later growth stages [32]. In addition, the imposed uniform increases in hydraulic conductivities and improvement of lymphatic functions across the entire tumor may not be realistic due to a lack of experimental data. The transvascular permeabilities of capillary and lymphatic vessel surfaces are assumed to be unchanged within the time frame in the current study. Our previous in vivo experimental results [19] showed sustained IFP reduction over 24 h post whole body heating; however, a study by Stapleton et al. [14] reported quick IFP recovery to its pre-heating level within 2 h after a local heating of 20 min. All those experimental results suggest complicated transport dynamics post heating. Further, as shown in the model, nanoparticle diffusion is at least an order of magnitude smaller than advection or depositions on cell surfaces; one would expect a shallow penetration depth from the capillaries in the interstitial space. We speculate that the accumulation of nanoparticles near capillaries with time would potentially block transcapillary flow by reducing capillary membrane permeability. If this could be verified by experimental studies, the model prediction of the nanoparticle accumulation rate in this study would overestimate the values, but the comparison among the cases may still be reasonable.

Further, this study can be considered a case study to investigate whether the proposed mechanisms lead to the observed nanoparticle deposition increase in PC3 tumors. The size used in the model was very similar to the PC3 tumors used in our in vivo experiments. The size of the gold nanoparticles with FAB attachments was used to determine the deposition rate coefficient to model particle attachment to the tumor. In addition, nanoparticle size can substantially affect the deposition rate coefficient, mainly through particle-surface interactions and the Brownian motion. Near the solid surface, the smaller the particle size, the stronger the effect of the adhesive van de Waals force and Brownian motion that drive the particle to migrate towards the surface. Both facilitate particle deposition on the solid surface and increase the deposition coefficient. Although the effects of the size and geometry selected in this study can be evaluated, it is not the main objective of the

current study. Simulation of the transport and deposition of nanoparticles of various sizes will be conducted in the future study. The model can be adapted easily by other researchers in the future when tumors/nanoparticles with specific size and geometry are investigated in animal or clinical settings to further understand contributions of possible transport mechanisms in those cancer treatment applications.

Another limitation of the theoretical model is on the prescribed time constant in describing nanoparticle concentration decay in capillary plasma. In principle, nanoparticle concentration decay in plasma is due to nanoparticles being captured by tumors and other organs in the body, including the liver, kidneys, and spleen. In fact, the percentage of nanoparticles captured by tumors is very small, typically less than 5% of the injected amount [2]. An ideal approach in simulation is to access experimental data of nanoparticle deposition rates in other organs in the body. The deposition rates in all the organs and tumors can then be implemented into a lumped system that only models the concentration decay with time while neglecting the spatial variation of nanoparticle concentrations in capillary plasma. Therefore, the lumped system analysis of the concentration decay could be incorporated into the developed theoretical model of nanoparticle transport in PC3 tumors to accurately predict nanoparticle deposition rate and amount in tumors. Unfortunately, biodistribution studies of nanoparticles in the mouse body were not performed in our experiments using PC3 tumors implanted in mice. We are expecting future improvements in simulation accuracy of our theoretical model with access to more experimental measurements.

5 Conclusions

The current study evaluates the roles played by improvement of hydraulic conductivity and lymphatic function in porous tumors on IFP reduction in tumors after whole body hyperthermia. The hydraulic conductivity of porous tumors K_t was first adjusted to match experimentally measured IFPs in PC3 tumors. Then, the enhanced hydraulic conductivity or functional lymphatic drainage in the tumor induced by heating demonstrated potential to lower tumor IFPs. It is evident that with higher nanoparticle extravasation due to lower IFPs and/or higher p_{blood} induced by whole body hyperthermia, nanoparticle concentrations are elevated in the tumor. This results in a more uniform nanoparticle distribution and larger overall nanoparticle accumulation rates in the tumor than that without heating. The resulting enhancement in nanoparticle deposition in PC3 tumors predicted by our theoretical model demonstrated an accumulation increase similar to that in our in vivo experiments. The current model can be further improved by adapting it to two- or three-dimensional analyses using realistic tumors and heterogeneous properties and by including realistic time-dependent nanoparticle concentration decay in blood plasma. We conclude that increases in the hydraulic conductivity and recovery of lymphatic functions are possible mechanisms that lead to IFP reductions and enhancement in nanoparticle deposition in PC3 tumors observed in our in vivo experimental studies.

Acknowledgments The research was performed in partial fulfilment of the requirements for the PhD degree in Mechanical Engineering by Manpreet Singh from the University of Maryland Baltimore County, Baltimore, Maryland, USA.

Funding This research was supported by a National Science Foundation research grant CBET-1705538.

References

1. Stylianopoulos T, Munn LL, Jain RK (2018) Reengineering the physical microenvironment of tumors to improve drug delivery and efficacy: from mathematical modeling to bench to bedside. Trends Cancer 4(4):292–319
2. Wilhelm S, Tavares AJ, Dai Q, Ohta S, Audet J, Dvorak HF, Chan WCW (2016) Analysis of nanoparticle delivery to tumours. Nat Rev Mater 1(5):1–12
3. Baish JW, Netti PA, Jain RK (1997) Transmural coupling of fluid flow in microcirculatory network and interstitium in tumors. Microvasc Res 53:128–141
4. Baxter LT, Jain RK (1989) Transport of fluid and macromolecules in tumors I. Role of interstitial pressure and convection. Microvasc Res 37:77–104
5. Koning GA, Eggermont AMM, Lindner LH (1750–1754) T.L.M ten Hagen, Hyperthermia and thermosensitive liposomes for improved delivery of chemotherapeutic drugs to solid tumors. Pharm Res 27(2010)
6. Ahmed M, Goldberg SN (2004) Combination radiofrequency thermal ablation and adjuvant IV liposomal doxorubicin increases tissue coagulation and intratumoural drug accumulation. Int J Hyperth 20:781–802
7. Osborne EJ, MacKillop WJ (1987) The effect of exposure to elevated temperatures on membrane permeability to adriamycin in Chinese hamster ovary cells in vitro. Cancer Lett 37:213–224
8. Kawai H, Minamiya Y, Kitamura M, Matsuzaki I, Hashimoto M, Suzuki H, Abo S (1997) Direct measurement of doxorubicin concentration in the intact, living single cancer cell during hyperthermia. Cancer 79:214–219
9. Merlin JL, Marchal S, Ramacci C, Notter D, Vigneron C (1993) Reversal of multidrug resistance by thermosensitive liposome-encapsulated doxorubicin combined with hyperthermia. Proc Ann Meeting Am Assoc Cancer Res 34:A1901
10. Toffoli G, Bevilacqua C, Franceschin A, Boiocchi M (1989) Effect of hyperthermia on intracellular drug accumulation and chemosensitivity in drug-sensitive and drug-resistant P388 leukaemia cell lines. Int J Hyperth 5:163–172
11. Leunig M, Goetz AE, Dellian M, Zetterer G, Gamarra F, Jain RK, Messmer K (1992) Interstitial fluid pressure in solid tumors following hyperthermia: possible correlation with therapeutic response. Cancer Res 52:487–490
12. Hauck ML, Dewhirst MW, Bigner DD, Zalutsky MR (1997) Local hyperthermia improves uptake of a chimeric monoclonal antibody in a subcutaneous xenograft model. Clin Cancer Res 3:63–70
13. Hauck ML, Coffin DO, Dodge RK, Dewhirst MW, Mitchell JB, Zalutsky MR (1997) A local hyperthermia treatment which

enhances antibody uptake in a glioma xenograft model does not affect tumor interstitial fluid pressure. Int J Hyperth 13:307–316
14. Stepleton S, Dunne M, Milosevic M, Tran CW, Gold MJ, Vedadi A, Mckee TD, Ohashi PS, Allen C, Jaffray DA (2018) Radiation and heat improve the delivery and efficacy of nanotherapeutics by modulating intratumoral fluid dynamic. ACS Nano 12:7583–7600
15. Lammers T, Peschke P, Kühnlein R, Subr V, Ulbrich K, Debus J, Huber P, Hennink W, Storm G (2007) Effect of radiotherapy and hyperthermia on the tumor accumulation of HPMA copolymer-based drug delivery systems. J Control Release 117:333–341
16. Li L, ten Hagen TLM, Bolkestein M, Gasselhuber A, Yatvin J, van Rhoon GC, Eggermont AMM, Haemmerich D, Koning GA (2013) Improved intratumoral nanoparticle extravasation and penetration by mild hyperthermia. J Control Release 167:130–137
17. Sen A, Capitano ML, Spernyak JA, Schueckler JT, Thomas S, Singh AK, Evans SS, Hylander BL, Repasky EA (2011) Mild elevation of body temperature reduces tumor interstitial fluid pressure and hypoxia and enhances efficacy of radiotherapy in murine tumor models. Cancer Res 71(11):3872–3880
18. Winslow TB, Eranki A, Ullas S, Singh AK, Repasky EA, Sen A (2015) A pilot study of the effects of mild systemic heating on human head and neck tumour xenografts: analysis of tumour perfusion, interstitial fluid pressure, hypoxia and efficacy of radiation therapy. Int J Hyperth 31:693–701
19. Gu Q, Liu S, Saha Ray A, Florinas S, Christie RJ, Daniel M-C, Bieberich C, Ma R, Zhu L (2020) Mild whole body hyperthermia induced interstitial fluid pressure (IFP) reduction and enhanced nanoparticle delivery to PC3 tumors: in vivo studies and MicroCT analyses. ASME J Therm Sci Eng Appl 12:061001(1-10)
20. Gu Q, Dockery L, Liu S, Daniel M-C, Bieberich C, Ma R, Zhu L (2019) Enhanced gold nanoparticle delivery to PC3 tumors by whole body hyperthermia using ICP-MS quantification of gold, Annual Meeting of the Biomedical Engineering Society (BMES) October 16-19. Philidiaphia, PA
21. El-kareh AW, Secomb TW (1995) Effect of increasing vascular hydraulic conductivity on delivery of macromolecular drugs to tumor cells. Int J Radiat Oncol Biol Phys 32(5):1419–1423
22. Su D, Ma R, Salloum M, Zhu L (2010) Multi-scale study of nanoparticle transport and deposition in tissues during an injection process. Med Biol Eng Comput 48:853–863
23. Stapleton S, Milosevic M, Allen C, Zheng J, Dunne M, Yeung I, Jaffray DA (2013) A mathematical model of the enhanced permeability and retention effect for liposome transport in solid tumors. PLoS ONE 8(12):e81157. https://doi.org/10.1371/journal.pone.0081157
24. Chakraborty S, Ozkan A, Rylander MN, Woodward WA, Vlachos P (2019) Mixture theory modeling for characterizing solute transport in breast tumor tissues. J Biol Eng 13(46):1–16
25. Truskey GA, Yuan F, Katz DF (2009) Transport phenomena in biological systems, 2nd Edition. Prentice Hall, Upper Saddle River
26. Khaled A-RA, Vafai K (2003) The role of porous media in modeling flow and heat transfer in biological tissues. Int J Heat Mass Transf 46(26):4989–4500
27. Ma R, Su D, Zhu L (2012) Multiscale simulation of nanoparticle transport in deformable tissue during an infusion process in hyperthermia treatments of cancers. In: Minkowycz WJ, Sparrow E, Abraham JP (eds) Nanoparticle Heat Transfer and Fluid Flow, Computational & Physical Processes in Mechanics & Thermal Science Series, vol 4. CRC Press, Taylor & Francis Group. https://doi.org/10.1201/b12983-4
28. Hoshyar N, Gray S, Han H, Bao G (2016) The effect of nanoparticle size on in vivo pharmacokinetics and cellular interaction. Nanomedicine 11(6):673–692
29. Moghadam MC, Deyranlou A, Sharifi A, Niazmand H (2015) Numerical simulation of the tumor interstitial fluid transport: consideration of drug delivery mechanism. Microvasc Res 101:62–71
30. Pishko GL, Astary GW, Mareci TH, Sarntinoranont M (2011) Sensitivity analysis of an image-based solid tumor computational model with heterogeneous vasculature and porosity. Ann Biomed Eng 39(9):2360–2373
31. Schuff MM, Gore JP, Nauman EA (2013) A mixture theory model of fluid and solute transport in the microvasculature of normal and malignant tissues. II: factor sensitivity analysis, calibration, and validation. J Math Biol 67:1307–1337
32. Zhang A, Mi X, Yang G, Xu LX (2009) Numerical study of thermally targeted liposomal drug delivery in tumor. ASME J Heat Transfer 131(4):043209
33. Curti BD, Urba WJ, Alvord WG, Janik JE, Smith JW 2nd, Madara K, Longo DL (1993) Interstitial pressure of subcutaneous nodules in melanoma and lymphoma patients: changes during treatment. Cancer Res 53:2204–2207
34. Milosevic M, Fyles A, Hedley D, Pintilie M, Levin W, Manchul L, Hill R (2001) Interstitial fluid pressure predicts survival in patients with cervix cancer independent of clinical prognostic factors and tumor oxygen measurements. Cancer Res 61:6400–6405
35. Zhu L (2010) Recent developments in biotransport. ASME J Thermodyn Sci Eng Appl 2(4):040801(1-11)
36. Heldin CH, Rubin K, Pietras K, Ostman A (2004) High interstitial fluid pressure — an obstacle in cancer therapy. Nat Rev 4:806–813
37. Willett GG, Boucher Y, di Tomaso E, Duda DG, Munn LL, Tong RT, Chung DC, Sahani DV, Kalva SP, Kozin SV, Mino M, Cohen KS, Scadden DT, Hartford AC, Fischman AJ, Clark JW, Ryan DP, Zhu AX, Blaszkowsky LS, Chen HX, Shellito PC, Lauwers GY, Jain RK (2004) Direct evidence that the VEGF-specific antibody bevacizumab has antivascular effects in human rectal cancer. Nat Med 10:145–147
38. Pietras K, Rubin K, Sjöblom T, Buchdunger E, Sjöquist M, Heldin C-H, Östman A (2002) Inhibition of PDGF receptor signaling in tumor stroma enhances antitumor effect of chemotherapy. Cancer Res 62:5476–5484
39. Berg A, Ekwall AK, Rubin K, Stjernschantz J, Reed RK (1998) Effect of PGE1, PGI2, and PGA analogs on EF2 collagen gel compaction in vitro and interstitial pressure in vivo. Am J Physiol 274:H663–H671
40. Mariana VF, Maria de Fátima GG, Maria P (2011) The effect of mechanical lymph drainage accompanied with heat on lymphedema. J Res Med Sci 16(11):1448–1451
41. Swartz MA, Lund AW (2012) Lymphatic and interstitial flow in the tumour microenvironment: linking mechanobiology with immunity. Nat Rev Cancer 12:210–219
42. Pathak AP, Artemov D, Neeman M, Bhujwalla ZM (2006) Lymph node metastasis in breast cancer xenografts is associated with increased regions of extravascular drain, lymphatic vessel area, and invasive phenotype. Cancer Res 66(10):5151–5158
43. Singh M, Gu Q, Ma R, Zhu L (2020) Heating protocol design affected by nanoparticle redistribution and thermal damage model in magnetic nanoparticle hyperthermia for cancer treatment. ASME J Heat Transfer 142(7):072501(1-9)

Manpreet Singh is currently a Ph.D. student in the Department of Mechanical Engineering at the University of Maryland Baltimore County, Baltimore, Maryland, USA. He received his master's degree in Engineering with distinction from Thapar Institute of Engineering and

Technology University, Patiala, Punjab, India, in 2016, and his bachelor's degree in Mechanical Engineering with distinction from Guru Nanak Dev Engineering College, Ludhiana, Punjab, India, in 2012. His research interests include image-based computational modeling approach to plan, develop, and optimize protocols in clinical hyperthermia or hypothermia therapies.

Dr. Ronghui Ma received her Ph.D. in Mechanical Engineering from State University of New York at Stony Brook in 2003. Her research focuses on computational and experimental study of transport phenomena such as fluid dynamics, multiphase heat and mass transfer, chemical reactions, and phase change involved in biomedical applications and material processing. She has more than 20 years' experience of numerical study of fluid dynamics and heat and mass transfer in complex systems. Specifically, she has conducted multiscale modeling of nanoparticle transport in and interactions with complex and deformable porous structures such as tumor tissue. Currently, she is an Associate Professor of Mechanical Engineering at the University of Maryland Baltimore County.

Dr. Liang Zhu received her B.S. in Mechanical Engineering at the University of Science and Technology of China, Hefei, China, in 1988, and her Ph.D. in Engineering at the City University of New York. She has been a faculty member at the University of Maryland Baltimore County (UMBC) since 1998. Currently, she is a Professor of Mechanical Engineering at UMBC. Her research interests include heat and mass transport in biological systems with emphases on clinical applications.